Chapter 6

Nonuniform global feedback

In the case of uniform global feedback, the control signal is generated from the spatial average of a system variable. However, if spatially nonuniform patterns emerge, the spatial average provides a response that is not at all specific to the type of pattern in the system. Obviously, different ways of computing a global feedback signal can be imagined that are more sensitive to the characteristic features of the patterns. The application of image processing and pattern recognition techniques opens many different directions for guiding spatiotemporal pattern formation in extended systems. In the following, a first step along this road is presented. By use of Fourier transform, a feedback protocol is defined that is sensitive to the presence of coherent structures in the medium. In Section 6.1, the feedback scheme is introduced. Experimental results from its application to catalytic CO oxidation on Pt(110) are shown in Section 6.2[1] and complemented with numerical simulations of the realistic reaction model for catalytic CO oxidation in Section 6.3. A discussion of the obtained results is presented in Section 6.4.

6.1 General remarks

In this chapter, pattern formation in catalytic CO oxidation on Pt(110) is studied in the excitable regime. In excitable media, previous efforts were directed at controlling the behavior of individual coherent structures that can be considered as basic build-

[1] The experiments were performed in collaboration with Md. Golam Moula

ing blocks of more complex spatiotemporal patterns. By introducing global feedback, traveling spots near the onset of translational motion could be stabilized. Collisions and scattering interactions of such objects as well as their transition to propagating wave patterns were studied [222]. Also, the dynamics of rotating spiral waves in confined geometries could be manipulated by global feedback [223]. In experiments with the photosensitive Belousov-Zhabotinsky reaction, stabilization of traveling wave fragments was achieved by globally controlling the excitability of the medium [224] and complex individual and collective motion of such fragments in the presence of spatial excitability gradients could be observed [40].

Here, a global feedback scheme is introduced that is sensitive to the length scales of the patterns emerging in the medium. In a chemical reaction-diffusion system, this type of control can be implemented in the following way,

$$\partial_t \mathbf{c} = \mathbf{f}(\mathbf{c}, q(t)) + \mathbf{D}\nabla^2 \mathbf{c} \tag{6.1}$$

$$q(t) = q_0 + \mu\,|\widehat{c}_i^{\mathbf{k}}(t-\tau)| \qquad \text{with} \qquad \widehat{c}_i^{\mathbf{k}} = \frac{1}{S}\int_S e^{-\mathrm{i}\mathbf{k}\mathbf{r}} c_i(\mathbf{r},t)\mathrm{d}\mathbf{r}\,, \tag{6.2}$$

where $\mathbf{c} = (c_1, c_2, ..., c_N)$ denotes the concentrations of reacting species with the diffusion matrix $\mathbf{D}$. The nonlinear functions $\mathbf{f}(\mathbf{c}, q)$ account for the reaction kinetics and depend on some global parameter q like temperature or pressure. The feedback signal is computed from the spatial distribution of one of the reacting components, c_i. It is chosen proportional to the modulus of a Fourier coefficient from the spectrum of the distribution of c_i and thus selectively depends on the length scales of the patterns in the system. In Fig. 6.1, this procedure is displayed schematically. For $k \equiv |\mathbf{k}| \neq 0$, a non-zero feedback signal is generated only if spatially nonuniform structures are

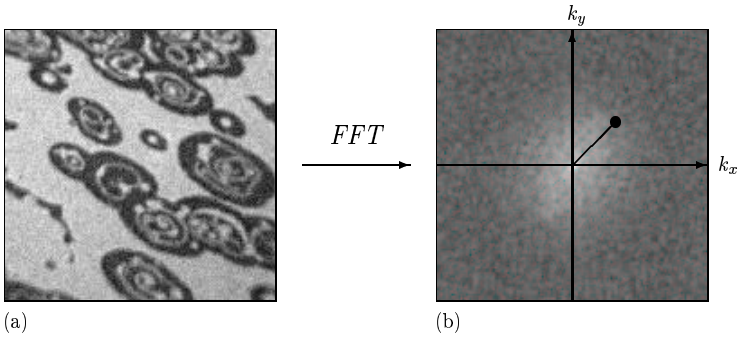

Figure 6.1: Nonuniform feedback. (a) PEEM image $I(x, y)$ and (b) its Fourier transform. The frequency image (b) is displayed as $\ln|\widehat{I}(k_x, k_y)|$. The filled circle schematically indicates the choice of the wavevector in the feedback scheme.

present in the medium. Therefore, in contrast to feedback signals that are computed from the spatial average of a system variable ($k = 0$, uniform feedback), the present coupling method does not ultimately drive the system to a uniform state but is expected to stabilize, within a large interval of feedback intensities μ, a situation where spatial patterns prevail. This control scheme will be referred to as *nonuniform* global feedback since it is sensitive to the presence of spatially nonuniform structures. In the following, nonuniform feedback is applied to catalytic CO oxidation on Pt(110) in both experiments and numerical simulations.

6.2 Experimental results

In this section, the dynamics of excitable catalytic CO oxidation under nonuniform global feedback is studied experimentally. The same setup as in the previous experiments with uniform feedback is used (for details on the setup see Section 2.2.5). Also in this case, the feedback is implemented globally by controlling the CO partial pressure in the reaction chamber (for general aspects of global control in catalytic CO oxidation see Section 4.1.1). The control signal is generated according to Eqs. (6.1) and (6.2). At each instant in time, a two-dimensional Fast Fourier Transform (FFT) is applied to the PEEM image $I(x, y)$. The feedback signal is then computed from the modulus of a Fourier coefficient $\widehat{I}^{\mathbf{k}}$ in the frequency plane of the image, the wave vector $\mathbf{k} = (k_x, k_y)$ being a feedback parameter. The value of the Fourier coefficient is averaged over a 3×3 pixel region at the tip of the wave vector and the choice of $\mathbf{k}$ is restricted to the diagonal of the upper right quadrant of the frequency plane ($k_x = k_y$ and positive), so that $\widehat{I}^{\mathbf{k}}$ is uniquely defined by fixing $k = \sqrt{k_x^2 + k_y^2}$. The feedback signal is scaled by an intensity factor μ and coupled back to the system as a modulation of the CO partial pressure in the reactor,

$$p_{\mathrm{CO}}(t) = p_{\mathrm{CO}}^0 + \mu |\widehat{I}^k(t - \tau)| \,, \tag{6.3}$$

where p_{CO}^0 is the base CO partial pressure. Besides, $\tau = \tau_i + \tau_{ext}$ denotes an effective control loop latency that consists of an externally chosen delay τ_{ext} and a minimal intrinsic time lag τ_i determined by the finite pumping rate of the reactor (in the present experiments, τ_i was of the order of one second).

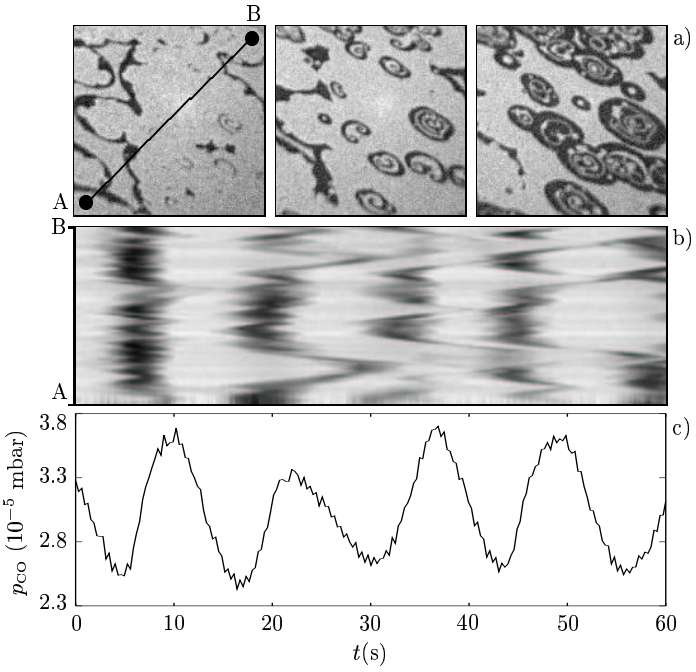

Figure 6.2: Pattern formation in the presence of nonuniform feedback. (a) PEEM images of typical patterns during one evolution cycle. (b) Space-time diagram along the diagonal AB indicated in the first snapshot in (a). (c) Evolution of CO partial pressure in the reactor. The parameters are $T = 453$ K, $p_{O_2} = 4 \times 10^{-4}$ mbar, $p^0_{CO} = 2.28 \times 10^{-5}$ mbar, $\mu = 1.54 \times 10^{-5}$ mbar, $k = 17.0$, and $\tau_{ext} = 0$ s [225].

Experiments were carried out in the excitable regime. Initiated at surface defects, traveling oxygen pulses, spiral fragments, and target waves can be observed on a mostly CO covered surface of the unperturbed system. If the feedback is set into action, a cyclic behavior is rapidly established in the system: bubble shaped oxygen islands repeatedly grow and get suppressed with a period of the order of ten seconds. Figure 6.2 (a) presents a series of three consecutive PEEM images showing typical concentration patterns emerging during one such cycle. In Fig. 6.2 (b), a space-time diagram is displayed, taken along the line AB indicated in the first snapshot in (a). The alternating dark and bright zones clearly reflect the oscillating evolution of patterns on the catalytic surface. The corresponding evolution of CO partial pressure is plotted in Fig. 6.2 (c).

In a series of experiments, the overall behavior of these pattern formation cycles was studied by systematic variation of the feedback intensity μ and the delay time τ_{ext}. Figure 6.3 (a) shows that the period T of oscillations in CO partial pressure decreases with increasing feedback intensity μ. However, for large μ this effect becomes less pronounced and the period levels off at some minimal value. For variation of the delay time τ_{ext} an opposite effect is observed. As τ_{ext} is increased, the period of oscillations grows monotonously, see Fig. 6.3 (b).

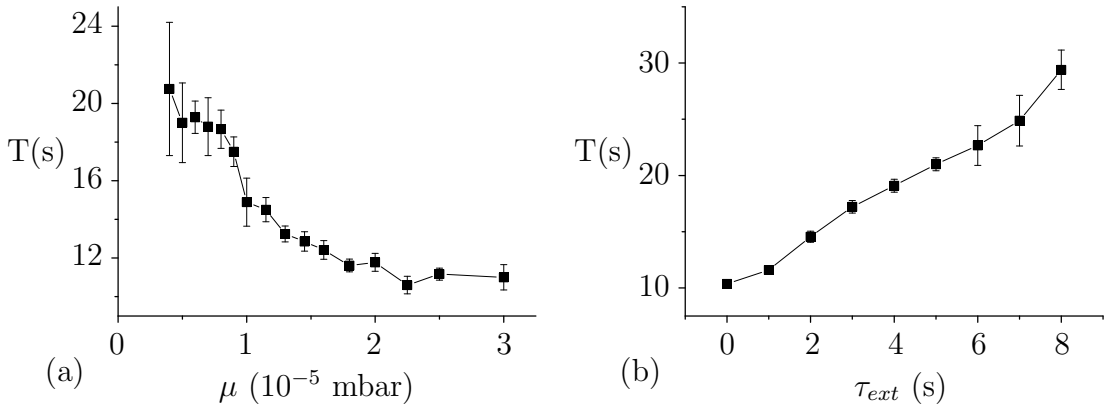

Figure 6.3: Period of pattern formation cycles as a function of (a) the feedback intensity μ and (b) the delay time τ. Parameters: (a) $T = 473$ K, $p_{O_2} = 4 \times 10^{-4}$ mbar, $p^0_{CO} = 4.33 \times 10^{-5}$ mbar, $k_x, k_y = 10$, $\tau_{ext} = 1$ s, (b) $T = 449$ K, $p_{O_2} = 4 \times 10^{-4}$ mbar, $p^0_{CO} = 2.28 \times 10^{-5}$ mbar, $k_x, k_y = 6$, $\mu = 1.54 \times 10^{-5}$ mbar [225].

Moreover, evidence is found that the characteristic size of the patterns depends on the modulus k of the wave vector. Figure 6.4 (a)–(d) shows bubble shaped objects typically observed under the effect of nonuniform feedback for different values of k. These oxygen patterns periodically grow and get erased by extending CO covered areas from the inside. To be able to compare different measurements, it is necessary to consider images at equivalent points of such pattern formation cycles. Therefore, the snapshots displayed in Fig. 6.4 (a)–(d) are taken when the feedback signal reaches its maximum. Obviously, the characteristic size of oxygen islands grows with increasing k from Fig. 6.4 (a) to (d). Also, the period of oscillations in CO partial pressure grows for larger values of k, see Fig. 6.5.

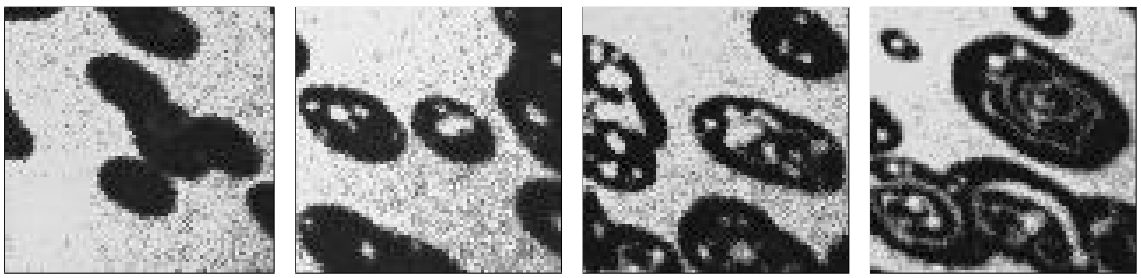

Figure 6.4: Size of patterns in the experiment for varying length k of the wave vector, $k_x, k_y = 6$ (a), 8 (b), 10 (c), and 12 (d). Experimental parameters as in Fig. 6.2 [225].

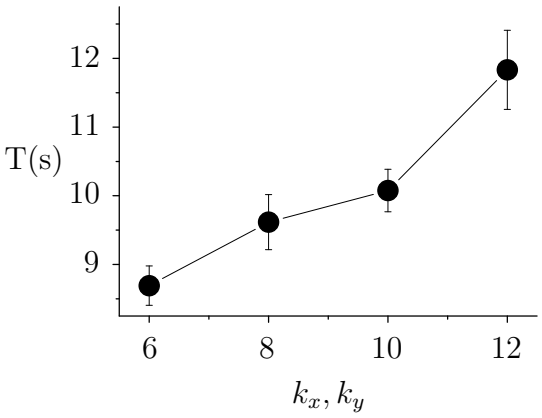

Figure 6.5: Dependence of the period of CO partial pressure oscillations on k. Parameters: $T = 449$ K, $p_{O_2} = 4\times10^{-4}$ mbar, $p^0_{CO} = 2.76\times 10^{-5}$ mbar, $\mu = 1.66 \times 10^{-5}$ mbar, $\tau_{ext} = 0$ s [225].

6.3 Numerical simulations

Numerical simulations were performed to support the experimental results. The computations are based on the realistic reaction model of catalytic CO oxidation on Pt(110) that was introduced in Section 2.2.4. Here, not only temporal phenomena but also the dynamics of spatial structures is of interest. Therefore, space dependence of the dynamical variables has to be taken into account. Spatial coupling is established by surface diffusion of CO [49, 141, 143], so that the model Eqs. (2.7)–(2.9) now read

$$\partial_t u = k_1\, p_{CO}\, s_{CO}(1-u^3) - k_2 u - k_3 uv + D\nabla^2 u \tag{6.4}$$

$$\partial_t v = k_4\, p_{O_2}[s_{O,1\times1} w + s_{O,1\times2}(1-w)](1-u-v)^2 - k_3 uv \tag{6.5}$$

$$\partial_t w = k_5 \left(\frac{1}{1+\exp\left(\frac{u_0-u}{\delta u}\right)} - w \right) . \tag{6.6}$$

The variables u, v, and w denote the CO coverage, the O coverage, and the local fraction of the catalyst surface in the nonreconstructed 1×1 phase, respectively. For a detailed explanation of the different terms see Section 2.2.4. In the following, Eqs. (6.4)–(6.6) are extended by a feedback mimicking the experimental setup of the previous section: the CO partial pressure p_{CO} is changing in time depending on the modulus of a chosen Fourier coefficient from the current spatial frequency spectrum of the CO coverage,

$$p_{CO}(t) = p^0_{CO} + \mu|\widehat{u}^k(t-\tau)| . \tag{6.7}$$

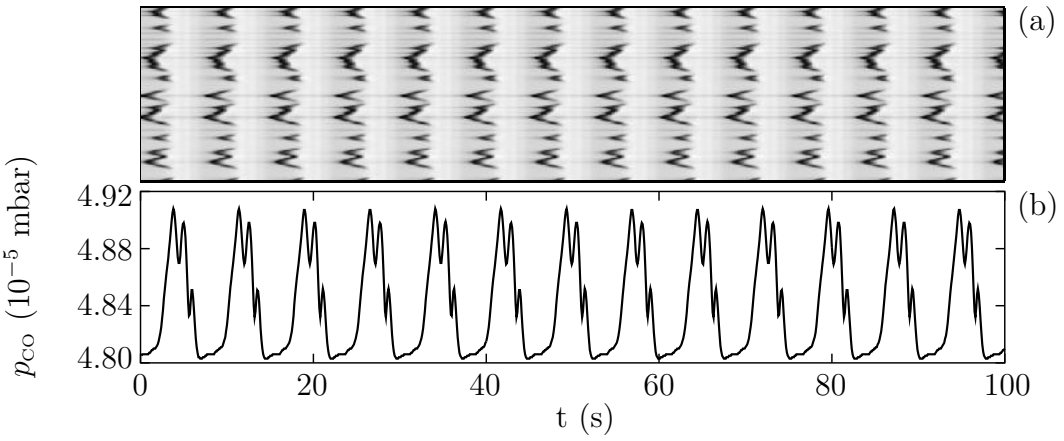

Figure 6.6: Pattern formation in the presence of nonuniform feedback in numerical simulations. (a) Space-time diagram and (b) evolution of CO partial pressure. Model parameters: $k_1 = 3.14 \times 10^5$ s^{-1} mbar^{-1}, $k_2 = 10.23$ s^{-1}, $k_3 = 283.9$ s^{-1}, $k_4 = 5.86 \times 10^5$ s^{-1} mbar^{-1}, $k_5 = 1.61$ s^{-1}, $s_{CO} = 1.0$, $s_{O,1\times1} = 0.6$, $s_{O,1\times2} = 0.4$, $u_0 = 0.35$, $\delta u = 0.05$, $D = 40\,\mu$m^2 s^{-1}, $p^0_{CO} = 4.8 \times 10^{-5}$ mbar, $p_{O_2} = 1.2 \times 10^{-4}$ mbar, and $T = 543.5$ K. Feedback parameters: $\mu/p^0_{CO} = 0.01$, $k = 10$, and $\tau = 3$ s. Numerical parameters: system length $L = 800\,\mu$m (1D, periodic boundaries), 200 grid points, and time step $\Delta t = 0.001$ s [225].

Following Section 5.1.2, Eq. (5.9), the spatial distribution of the CO coverage u is used to approximate the image intensity I for the generation of the feedback signal. All simulations are performed in the excitable regime. The numerical and model parameters can be found in the caption of Fig. 6.6. The presence of surface defects is modeled by an increased oxygen sticking probability. This approach is inspired by observations from scanning tunneling microscopy that show a strain induced increase in the probability of dissociative adsorption in the vicinity of defects for both oxygen [226] and NO [227] on Ru(0001). It is assumed that the dissociative adsorption of oxygen on the Pt(110) surface is similarly enhanced by the presence of defects. For the simulations shown in Figs. 6.6 and 6.7, surface defects are introduced as follows. The locations of defects are chosen by a random number generator that produces uniformly distributed integer random numbers in the interval $[0, N-1]$ with $N = 200$ the number of grid points. From this interval, 40 random numbers are drawn and taken as the position of defects. At these positions, the oxygen sticking coefficients on both the (1×1) and the (1×2) structure are increased by a value between zero and 0.04 (the exact increase at each defect is chosen by a random number generator from the interval $[0, 0.04]$).

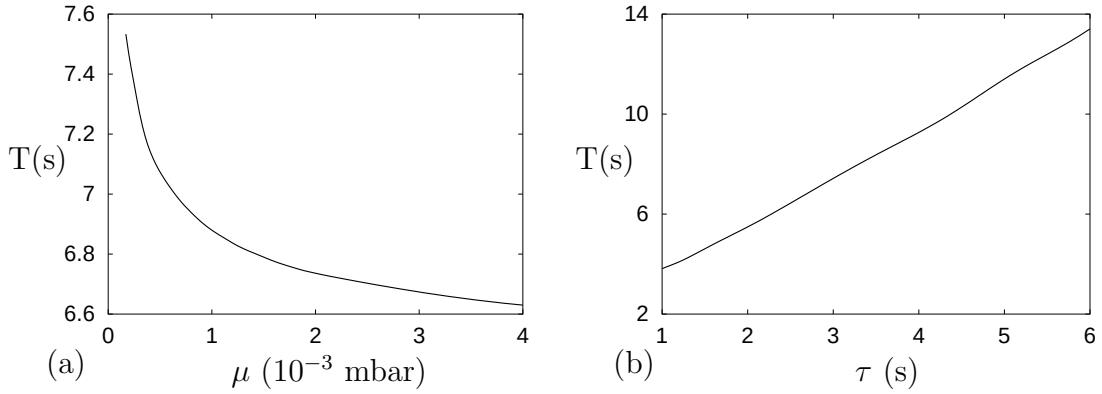

Figure 6.7: Period of pattern formation cycles as a function of (a) the feedback intensity μ and (b) the delay time τ in numerical simulations. For model and numerical parameters, see Fig. 6.6. Feedback: (a) $\tau = 3$ s, (b) $\mu = 2 \times 10^{-4}$ mbar, and (a), (b) $k = 10$ [225].

Figure 6.6 shows the space-time diagram (a) and the evolution of CO partial pressure (b) of a typical model simulation in the presence of nonuniform global feedback. A cyclic behavior qualitatively similar to the experimental results is observed: starting from surface heterogeneities, patterns repeatedly emerge and get suppressed by the feedback. The period of oscillations in CO partial pressure is of the same order as in the experiment.

Also for the period T of pattern formation cycles a dependence on the feedback parameters similar to the experiment is found. Figures 6.7 (a), (b) and Fig. 6.8 show numerical results of systematic scans of the feedback intensity, the delay time, and the wave number k corresponding to the experimental results in Figs. 6.3 (a), (b) and Fig. 6.5. As in the experiment, the period of oscillations is reduced for increasing feedback intensity μ and grows with increasing control loop latency τ and with increasing wave number k.

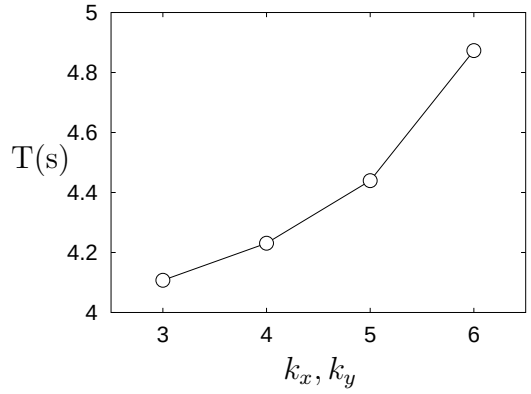

Figure 6.8: Dependence of the period of CO partial pressure oscillations on k in numerical simulations. 2D system with periodic boundaries, L^2 with $L = 400\,\mu$m (100×100 grid points). $s_{\mathrm{O},1\times1/1\times2}$ are increased by 0.04 in a region of 3×3 grid points at the center. Parameters: $\mu/p^0_{\mathrm{CO}} = 0.06$, $\tau = 1$ s, other numerical and model parameters as in Fig. 6.6 [225].

6.4 Discussion

In previous approaches to control pattern formation in excitable systems, feedback signals were computed from an averaged system variable [222,223]. With respect to these methods, nonuniform feedback can be regarded as a more general form that comprises the earlier work as the particular situation where $k = 0$. In the case considered here ($k \neq 0$), the feedback is sensitive to the presence of spatially nonuniform structures and becomes active only if the system shows patterns that contain the respective mode in their frequency spectrum.

In the parameter regime of the above experiments, an irregular distribution of oxygen pulses and wave fragments, triggered at surface defects and moving on an otherwise CO covered surface, prevails. Since in general these objects do not form a regular periodic structure, the frequency spectrum exhibits a broad band of active modes. If k is chosen to be roughly of the same order as the overall length scale of the patterns it can be expected to lie within this band of active modes. Thus, if patterns emerge in the system, the coupling will respond with an increase in CO partial pressure which counteracts the further growth of oxygen patterns and, therefore, can be regarded as a negative feedback. It induces a periodic behavior of the reaction depending, of course, on the delay in the control loop: oxygen patterns emerge, the feedback becomes active, and the CO partial pressure increases, so that the patterns get suppressed, the feedback signal vanishes, the CO pressure drops, and again patterns can start to emerge.

This scenario offers a rationalization of the results presented above. For larger feedback intensities μ the emergence of patterns leads to a steeper increase in CO partial pressure. Patterns then get erased more rapidly and the period of the cyclic pattern evolution becomes shorter as was shown in Fig. 6.3 (a) and Fig. 6.7 (a). However, for large μ the feedback signal almost instantaneously crosses the p_{CO} level where oxygen patterns get suppressed so that a continuing increase in μ does not shorten the response time of the coupling scheme any further and the period converges to a minimum value. An increasing delay in the feedback loop simply extends the interval between the emergence of patterns and the response of the coupling scheme so that the overall period of the oscillatory cycles grows linearly as can be seen in Fig. 6.3 (b) and Fig. 6.7 (b). Within some interval of k values, both experiments and numerical simulations show

a growing period for increasing k, see Fig. 6.5 and Fig. 6.8. Within this range, the coefficients in the frequency spectrum are decaying for larger k, which corresponds to a decreasing feedback intensity and is thus consistent with the results shown in Fig. 6.3 (a) and Fig. 6.7 (a). Since the final size of the oxygen islands depends on the time interval during which they can grow, large structures are observed for longer periods T and hence for increasing k.